Published in final edited form as:
Neurobiol Aging. 2010 February ; 31(2): 244–256. doi:10.1016/j.neurobiolaging.2008.03.013.

White Matter Pathology Isolates the Hippocampal Formation in Alzheimer's Disease

DH Salat[*,a,c], **DS Tuch**[a], **AJW van der Kouwe**[a], **DN Greve**[a], **V Pappu**[a,b], **SY Lee**[a,b], **ND Hevelone**[a,b], **AK Zaleta**[a,b], **JH Growdon**[b], **S Corkin**[a,c], **B Fischl**[a], and **HD Rosas**[a,b]

[a]MGH/MIT/HMS Athinoula A. Martinos Center for Biomedical Imaging, Charlestown MA and Department of Radiology, Massachusetts General Hospital, Boston MA

[b]Department of Neurology, Massachusetts General Hospital, Boston MA

[c]Department of Brain and Cognitive Sciences, Massachusetts Institute of Technology, Cambridge MA

Abstract

Prior work has demonstrated that the memory dysfunction of Alzheimer's disease (AD) is accompanied by marked cortical pathology in medial temporal lobe (MTL) gray matter. In contrast, changes in white matter (WM) of pathways associated with the MTL have rarely been studied. We used diffusion tensor imaging (DTI) to examine regional patterns of WM tissue changes in individuals with AD. Alterations of diffusion properties with AD were found in several regions including parahippocampal WM, and in regions with direct and secondary connections to the MTL. A portion of the changes measured, including effects in the parahippocampal WM, were independent of gray matter degeneration as measured by hippocampal volume. Examination of regional changes in unique diffusion parameters including anisotropy and axial and radial diffusivity demonstrated distinct zones of alterations, potentially stemming from differences in underlying pathology, with a potential myelin specific pathology in the parahippocampal WM. These results demonstrate that deterioration of neocortical connections to the hippocampal formation results in part from the degeneration of critical MTL and associated fiber pathways.

Keywords

Alzheimer; aging; diffusion tensor imaging; fractional anisotropy; diffusivity; MRI; white matter; dementia; hippocampus; entorhinal; memory; axial diffusivity; radial diffusivity; tractography; volume; hyperintensities; T2; myelin; axon

1. Introduction

Careful histological examination of the brains of individuals with Alzheimer's disease (AD) has uncovered a probable substrate for the memory impairment in this condition. Specifically, layer-preferred degeneration in perirhinal and entorhinal cortices likely impedes the transfer of information from the neocortex to the hippocampus [2,9,25,33,34,86], thereby degrading the processing and storage of sensory input. Layer II of the entorhinal cortex shows profound alterations, including substantial loss of neurons even

Corresponding Author: David H. Salat, Ph.D., MGH/MIT/HMS Athinoula A. Martinos Center for Biomedical Imaging, MGH Dept. Radiology, Building 149, 13th St., Mail Code 149 (2301), Charlestown, MA 02129-2060, Phone: 617-726-4704, Fax : 617-726-7422, salat@nmr.mgh.harvard.edu.

Disclosure Statement. There are no conflicts of interest.

in the early stages of AD [25]. The projection termination zone of these fibers in the dentate gyrus of the hippocampal formation is also marked by degenerative changes, effectively resulting in a 'disconnection' between association and limbic cortices [33,34]. Given these important pathologic signatures, the majority of studies of mechanisms of AD symptomology have focused on medial temporal lobe (MTL) cortical degeneration. Nevertheless, these prior findings also implicate regional connectivity as a factor contributing to cognitive deterioration. Histological research demonstrates that brain white matter (WM) also degenerates in AD [10,19,20,34]. Brun and Englund (1986) reported a syndrome in 60% of AD patients of demyelination and axonal and oligodendroglial loss with accompanying gliosis in the deep WM that was independent from gray matter lesions. The authors suggested that the degeneration was potentially due to comorbid factors such as hypertension [10]. WM disease, however, has been reported at autopsy in individuals with pure AD with no components of vascular brain disease [71]. Further, myelin staining is reduced in the perforant pathway, the main input fibers projecting neocortical information from the entorhinal cortex to the granule cells of the dentate gyrus in the hippocampal formation [34]. These findings suggest that at least some of the WM changes in AD are not due simply to comorbid factors, but are likely associated with AD pathological processes including MTL cortical pathology. The pathologic signatures spanning the perforant pathway, and the reduction in myelin integrity of this fascicle, underscores the potential influence of regional connectivity in the putative propagation of neurodegenerative events. An open question is whether such changes could be detected in patients *in vivo*, and whether this principal of degeneration in anatomically connected regions extends beyond the findings in the perforant pathway.

Neuroimaging studies have attempted to understand patterns and mechanisms of WM pathology in AD, and the clinical significance of such changes [17], but regional the patterns and potential mechanisms of this WM pathology are still unclear. Moreover, whether WM changes are independent of classically described AD cortical pathology, such as hippocampal atrophy, is completely unknown. Total and regional WM volume is reduced in AD [24,38,64–66,78], and WM signal abnormalities are associated with risk for cognitive decline [1] and dementia [57], as well as an enhanced clinical syndrome in specific cognitive domains [30]. The use of WM signal abnormalities as a clinically relevant measure of WM pathology remains controversial because a number of studies report little consequence of this marker on clinical status [51,70]. Additionally, WM volume measures are limited because of the need to define regionally identifiable borders using morphometric landmarks, a particularly difficult task given the complex anatomy of WM and the limited information provided about this anatomy from a standard structural MR image.

Diffusion tensor imaging (DTI) has been applied extensively to understand the regional basis of tissue degeneration in a variety of clinical conditions including the study of normal aging [50,53–55,67,68,79–81]. Two primary metrics of the diffusion properties within a voxel, termed diffusivity and fractional anisotropy (FA) [3,6,56], have been commonly employed as indices of tissue pathology. More recently, studies by Song and colleagues utilizing animal models demonstrate that the diffusivity measure can be further subdivided in to axial and radial components, which could provide information on axonal and myelin pathology selectively [11,74,75]. Rose and colleagues [61] demonstrated altered diffusion measures in the splenium of the corpus callosum, the superior longitudinal fasciculus, cingulum, and internal capsule in patients with AD, and in parahippocampal, thalamic, and cingulate WM in individuals with mild cognitive impairment [62]. Diffusion measures were related to indices of disease severity and cognitive ability and the specific association with episodic memory presents a potential clinical role for DTI to index WM degeneration and track AD symptoms. Other studies have found altered diffusion measures in patients with AD in the uncinate and inferior occipital fasciculi [83], and in the corpus callosum and WM

of the frontal, temporal, and parietal lobes [8]. Two studies in AD [28,45] demonstrated generalized alterations in diffusion measures of posterior lobar WM that differed from those seen in normal aging. Two recent studies provide preliminary investigation into mechanisms of WM alteration in AD through the examination of axial and radial diffusivity [14,31]. These studies examined selected regions of interest in small participant samples (10 AD in the former, and 6 AD in the latter study), and reached different conclusions with one focusing on compromised myelin [14] and the other suggesting loss of axonal processes as a primary pathologic mechanism [31]. These prior studies provide important information about the regional patterns of AD pathology, yet questions remain about the whole brain patterns of WM change in these various diffusion parameters in AD. Additionally, no prior study has examined how classically described measures of pathology such as white matter signal abnormalities and hippocampal atrophy contribute to the changes measured.

The current study aimed to elucidate regional patterns of alterations in diffusion parameters in AD through a comprehensive, whole brain analysis of commonly and recently described DTI measures of tissue integrity. These analyses included the examination of anisotropy and axial and radial diffusivity components, and whether changes in these diffusion parameters provide information beyond traditional MRI measures of gray and WM degeneration. We used recently developed procedures in the FSL image analysis suite (http://www.fmrib.ox.ac.uk/fsl/) for interparticipant registration, reducing potential confounds in spatial normalization. We additionally utilized tractography procedures to define a path of interest (POI) in the native space of each individual to confirm voxel-based results. We find complex regional patterns of alterations in diffusion parameters with AD, with prominent changes in pathways associated with the hippocampal formation. These changes are beyond what can be explained by classically described AD pathology, and suggest that multiple pathologies may disrupt the transfer of neocortical information to limbic structures important for a range of cognitive processes.

2. Methods

2.1 Participants

Images were obtained for 74 participants (Table 1). 20 patients with probable Alzheimer's disease (AD, mean age 77.8±4.9 years) were recruited through the Massachusetts General Hospital Memory Disorders Unit (MGH-MDU) and 54 non-demented older adults (OA, mean age 75.8±5.6 years) through the Harvard Cooperative Program on Aging (http://www.hebrewrehab.org/home_institute.cfm?id=90) and the Nurses' Health Study (http://www.channing.harvard.edu/nhs/) at Harvard Medical School and Brigham and Women's Hospital. OA were screened for dementia using one of the following mental status examinations: the Mini Mental Status Exam (MMSE) [23], the Blessed Dementia Scale (BDS) [7,76], or the Telephone Interview of Cognitive Status (TICS) [16,41]. AD patients were assessed by the Clinical Dementia Rating scale (CDR) [32,48,49] which yields a calculated global score (CDR rating) as well as a summated score of individual CDR domains (sum of boxes). All patients with AD were assessed by a memory disorders neurologist from the MGH-MDU. AD diagnoses as determined by CDR score were very mild to mild AD in 90% and moderate dementia in 10%. Participants were excluded if they had a history of significant neurologic or psychiatric disorder (other than AD), or serious cerebrovascular conditions. Groups were matched for proportion of individuals with controlled elevated blood pressure.

2.2. DTI acquisition

Global and regional WM integrity was assessed using DTI measures of FA and diffusivity (comprised of axial and radial components [11,74,75]), as well as through T2 image

intensity. Image acquisition employed single shot echo planar imaging with a twice-refocused spin echo pulse sequence, optimized to minimize eddy current-induced image distortions [58] (Siemens Avanto; TR/TE=7400/89 ms, b=700 s mm-2, 256×256 mm FOV, 128×128 matrix, 2 mm slice thickness with 0-mm gap, 10 T2 + 60 DWI, total acquisition time 8 min 38 sec). We acquired 64 slices in the AC-PC plane. The 60 diffusion weighted directions were obtained using the electrostatic shell method [39], providing a high signal-to-noise diffusion volume. The diffusion tensor was calculated on a voxel-by-voxel basis with conventional reconstruction methods [5] using tools developed at the Martinos Center at MGH.

2.3 DTI preprocessing and analysis: Motion and eddy current correction

Image preprocessing was performed as described in our previous work [67,68]. Diffusion volumes were motion corrected and averaged using FLIRT (FMRIB's Linear Image Registration Tool; http://www.fmrib.ox.ac.uk/analysis/research/flirt/) [37] with mutual information cost function to register each direction to the minimally eddy current distorted T2-weighted DTI volume that had no diffusion weighting.

2.4 Fractional anisotropy (FA) and diffusivity map calculation

The primary measures acquired from the DTI data were two common scalar metrics describing the WM microstructure. FA, which is dependent on the orientational coherence of the diffusion compartments within a voxel [56], was considered the primary metric of interest given the use of this parameter in a number of recent studies of tissue deterioration. FA was calculated using the standard formula defined previously [4]. Diffusivity is a scalar measure of the total amount of diffusion within a voxel calculated as described in previous work [6]. We additionally examined measures of axial (λ_1) and radial [($\lambda_2 + \lambda_3$)/2] diffusivity as described in prior work [11,74,75]. T2 images were obtained using the exact parameters as the diffusion sensitive images except without any diffusion weighting. The T2 images were analyzed to determine whether changes other than those in tissue microstructure contributed to the observed effects because T2 differences would reveal technical artifact such as image registration or atrophy, as well as large scale signal changes such as WM signal abnormalities (e.g. hyperintensities).

2.5 Nonlinear registration and tract-based spatial statistics (TBSS). [63,72,73]

Voxelwise statistical analysis of the FA data was carried out using TBSS (Tract-Based Spatial Statistics [72]), part of FSL [73]. All participants' diffusion data were first aligned into a common space using the nonlinear registration IRTK [63] (www.doc.ic.ac.uk/~dr/software). Next, a mean FA image was created across all participants, and this mean image was thinned to create a mean FA skeleton which represents the centers of all tracts common to the group. Each participant’s aligned FA data were then projected onto this skeleton and the resulting data fed into voxelwise group statistics. Data along the skeleton were smoothed utilizing an anatomical constraint to limit the smoothing to neighboring data within adjacent voxels along the skeleton. All analyses were masked to only display regions with FA values of > 0.2 to avoid examination of regions that are likely comprised of multiple tissue types or fiber orientations. The exact transformations derived for the anisotropy maps were applied to the T2 and diffusivity volumes for matched processing of all image volumes. Statistical maps were dilated from the TBSS skeleton for visualization purposes.

2.6 Hippocampal, WM, and WM signal abnormality volume measurements

Hippocampal, WM, and WM signal abnormality volume measurements were calculated through an automated procedure, using probabilistic information estimated from a manually

labeled training set as described in our prior work [22,27,88]. All volumetric measures were corrected as a percentage of intracranial volume (ICV).

2.7 POI analyses

We created highly constrained region of interest measures in parahippocampal WM across multiple participants using a procedure termed POI to reconstruct optimal pathways from a DTI image. This procedure was performed to obtain native space measurements across individuals in a homologous region of WM spanning the anterior to posterior parahippocampal gyrus. This region is comprised of multiple important fiber systems, including the perforant pathway, the parahippocampal/cingulum fibers, and fibers projecting from the amygdala to the parahippocampal region (the anatomy of the cortical projections recently summarized in [47,69]). Anterior-posterior fiber systems dominate the tensor directionality in this region. However, it is important to note that additional fiber systems can contribute to the diffusion parameters of tissue integrity within this path. The POI was created by first transforming each participant's T2 and anisotropy maps to standardized space to facilitate identification of manually placed homologous initiation and termination points for the POI in each individual's DTI volume. Based on the tensor data, the optimal (strongest) path among all voxels in the labeled start and end points in the 3D volume was identified, and a path was created between those two points. FA was then sampled from the central voxels along the entire path, and the values were interpolated so that the number of samples along the path was the same across participants for point-by-point FA comparisons. Compared to region of interest approaches, the POI method allows sampling over extended WM pathways by simply specifying the initial and terminal points. The path construction algorithm is based on the replica exchange Monte Carlo (REMC) method [26,59,82], a recently developed improvement to the Metropolis-Hastings algorithm. The REMC algorithm operates by simulating multiple replica of the system simultaneously. Each system undergoes optimization according to the classical Metropolis-Hastings procedure, but the different replica can exchange temperatures through a Metropolis step. The multiple replica can search the configuration space efficiently, and the temperature exchange step enables the replica to overcome local minima. The REMC algorithm models the WM pathway as a trilinear spline with a sparse number of control points. The energy of the path is defined as the negative log product integral of the diffusion orientation distribution function [84] along the path (Figure 4). Data were smoothed using an anatomical constraint along the path by obtaining the mean of each set of three neighboring voxels.

3. Results

3.1 Voxel-based group comparisons of DTI measures

Figure 1 demonstrates a coronal slice showing the mean FA map of each group from the spatially normalized FA volumes using the IRTK nonlinear registration step [63] of the tract-based spatial statistics (TBSS) [72] procedure (top), and a representative individual FA map (bottom) from the OA (left) and the AD (right) groups. Importantly, much of the anatomic detail of the individual participant volumes was retained in this initial processing of the TBSS procedure.

Table 2 lists regions showing reduced FA in AD compared to OA without the use of any nuisance regressors. FA was reduced in numerous regions including bilateral reductions in lateral occipital WM, middle and inferior temporal WM, inferior parietal/supramarginal WM, precuneus WM, and parahippocampal WM. Figure 2 demonstrates the TBSS-based statistical comparison of FA and diffusivity between OA and AD controlling for T2 intensity at each voxel (Figure 2, left panel). When controlling for T2 intensity, changes in FA were most prominent in parahippocampal and temporal, precuneus, and ventromedial frontal WM

(Figure 2). Diffusivity increased with AD in regions similar to those reported for FA yet were somewhat more widespread with additional changes in the corpus callosum, cingulum, occipital, and periventricular regions. Overlap in FA and diffusivity changes (results with a *p* value of 0.01 or lower) was greatest in medial temporal, precuneus, and ventromedial frontal WM (Figure 2; bottom left panel). Analyses in Figure 2 controlled for T2 intensity at each voxel, and therefore the changes measured exceeded those of T2 which would be affected by partial volume and WM hyperintensities.

Increases were apparent in the radial as well as axial components of diffusivity (Figure 2, right panel) however, these components were affected in an almost completely regionally distinct manner. Increases in axial diffusivity were most apparent in periventricular, occipital, and callosal regions whereas increases in radial diffusivity were more selectively localized to medial temporal, occipital, and precuneus WM. Overlap of changes in the two components was in small portions of occipital and temporal WM (Figure 2, right panel, bottom).

3.2 Comparisons of DTI measures controlling for hippocampal volume and T2

Because hippocampal atrophy is a neuroimaging hallmark (although not perfectly specific) of AD degenerative processes [36], we next examined whether changes in the diffusion measures remained when controlling for hippocampal volume in addition to T2 intensity. Controlling for these parameters reduced the statistical effect on FA and diffusivity in certain areas including the precuneus and medial frontal WM (Figure 3). However, the statistical effect on temporal lobe WM, and in particular, temporal and parahippocampal WM remained. Differences in thalamic and internal capsule WM were also highlighted in this analysis. Overlap in changes in FA and in diffusivity was apparent in medial temporal, thalamic, and temporal stem and pyramidal WM when controlling for T2 and hippocampal volume. These results demonstrate that diffusion measures in these regions provide unique information compared to hippocampal volume and T2 signal intensity alone.

3.3 POI analysis

The results of the voxel-based analyses in parahippocampal WM were confirmed using the POI tractography technique to extract native space values from each individual. Figure 4 demonstrates this procedure and results from this analysis. FA was reduced in patients on a point-by-point basis along the majority of the path, confirming the findings from the voxel-based results with stronger effects in the more anterior portions of the pathway (the points on the right side of the plot; bottom panel). Total path length did not significantly differ between the two groups. Mean values of all points from along the path demonstrated highly significant reduction in FA (Figure 5). For comparison, the effects of AD on hippocampal volume, whole brain WM volume, and white matter signal abnormality volume [22,27,88] are also presented (Figure 5).

4. Discussion

These data demonstrate for the first time, the distinct and overlapping anatomy of whole brain changes in anisotropy and diffusivity, as well as the differential patterns of alterations in axial and radial diffusivity. These different diffusion parameters provide unique information, and the results demonstrate the complex anatomical basis of DTI changes in AD. To a certain extent, the most prominent regional tissue changes in overlapping diffusion parameters resembled the anatomic connectivity of MTL structures that are important for memory processes, with alterations in parahippocampal and ventromedial frontal WM. Of note were bilateral alterations in FA in the precuneus, which is connected to the MTL by way of retrosplenial cortex, and is considered by some to be part of the limbic system [12].

This region is of great current interest in the study of AD because the precuneus is likely an extension of the MTL memory system [87], and is functionally and structurally altered by AD pathology [29,35,44,46,60,89]. Several regions outside of this medial temporal network were also affected, however, including various portions of occipital, temporal, and parietal WM, and more minimal changes in frontal WM. Greater changes in radial compared to axial diffusivity were apparent in the parahippocampal WM, suggesting that the pathology in this region includes some form of myelin degradation and the current data demonstrate the first whole brain regional description of this effect.

Prior voxel-based morphometry studies have demonstrated alterations in parahippocampal WM in AD [77]. Our work is also in accord with previous work demonstrating altered diffusion properties in parahippocampal, thalamic, and cingulate WM [62] and in posterior lobar WM [28,45] in individuals with AD and mild cognitive impairment, suggesting that the changes measured here could be apparent in the earliest stages of AD. Rose and colleagues [62] suggested that changes in the left hemisphere were greater than those in the right hemisphere. These results are qualitatively supported by the POI analyses in the current study, demonstrating that although left and right parahippocampal WM are both affected in AD, the left path demonstrated more points reaching a statistical effect compared to the homologous region in the right hemisphere. Formal testing for laterality effects will be an important topic of future research. Additionally, the POI analyses suggest a potential anterior to posterior gradient of WM damage in the parahippocampal WM. Such a finding would have important implications for memory function as it is suggested that recollection, familiarity, and novelty are supported by different MTL subregions [15]. These data are also in accord with regional patterns recently presented in a study contrasting AD and cerebrovascular disease [13]. Altered DTI measures have been related to indices of disease severity and cognitive ability, with particular association with episodic memory, presenting a potential clinical role for DTI in uncovering WM degeneration in the clinical presentation of AD [62]. The present results demonstrate regional changes in parahippocampal and precuneus WM, and degeneration of these regions may result in isolation of the hippocampus from neocortical input and related areas that have been recently described to comprise part of a functional memory circuit [87].

The relation between DTI measures and more classical imaging indices of pathology, including brain volume, is not clear. Our prior volumetric work demonstrated significantly lower prefrontal WM volume in patients with AD compared to age-matched control participants [64], and the current data may suggest that this effect is due to degenerative changes in selective regions. The current data demonstrate that changes in diffusion metrics provide independent information beyond hippocampal volume alone. Removing variance due to hippocampal volume did not reduce the effects measured in parahippocampal WM, and even highlighted effects in thalamic regions that were less apparent in the group comparisons without consideration of hippocampal volume. The association between microstructural FA measures and macrostructural volumetric measures may be complex [68]. Similarly, the pathologic basis of changes in DTI measures is currently unknown. Prior studies report loss of oligodendrocytes, reactive astrocytosis, and reduction in neuropil density that could contribute to WM damage in AD [71], and we posit that at least some of the measured effects could be due to Wallerian degeneration of axons and the surrounding myelin sheath. However, that fact that effects remained in the MTL WM after regressing out hippocampal volume and that there was greater alteration in radial as opposed to axial diffusivity in parahippocampal WM supports prior work demonstrating reduced myelin staining in AD [34], and suggests that the effects measured are somewhat independent of regional cortical degeneration and may represent a unique myelin pathology [11,74,75]. These findings should be interpreted with caution however, as it is important to note that the current data also demonstrated a regional increase in axial diffusivity. This is not what is

expected from the animal models demonstrating that axonal pathology should result in a decrease in axial diffusivity [74], and little information exists for the interpretation of increased axial diffusivity. DTI has been used to guide pathology studies [21], and further work with similar methods will likely yield important new information about how these novel diffusion measures relate to histopathology in AD.

The current results have some limitations. The changes in FA measured were relatively small and regionally localized, and thus it is unknown how early such changes could be detected. Future work will examine individuals with mild cognitive impairment to determine whether the current pattern of results exist in preclinical stages of disease. Although advanced procedures were applied to address common concerns of diffusion imaging studies, further improvement is required in this field. Methods to enhance spatial [40,42,43] and angular [84,85] resolution will be necessary to fully exclude concerns about eddy current and susceptibility artifact distortions. Similarly, although the procedures used here are superior to standard linear transformations for registration of DTI data, the potential still exists for further refinement of DTI registration using the full tensor information [52]. In spite of these limitations, the current analysis procedures provide a set of techniques that address common concerns for the analysis of DTI data, and demonstrate the vulnerability of WM to AD pathology. Thus, along with cortical degeneration, we suggest that an additional mechanism underlying AD clinical symptoms is the WM degeneration that further isolates MTL structures.

Acknowledgments

This work was supported in part by NIH K01AG024898, a Massachusetts Alzheimer's Disease Research Center Pilot Grant 2001/2002 (AG05886), the National Center for Research Resources (P41RR14075), the Mental Illness and Neuroscience Discovery (MIND) Institute, and a grant from the National Alliance for Medical Image Computing (NAMIC U54 EB05149). We thank Dr. Francine Grodstein and the Nurses' Health Study for a portion of the participant recruitment and imaging.

References

1. Au R, Massaro JM, Wolf PA, Young ME, Beiser A, Seshadri S, D'Agostino RB, DeCarli C. Association of white matter hyperintensity volume with decreased cognitive functioning: the Framingham Heart Study. Arch Neurol 2006;63(2):246–250. [PubMed: 16476813]
2. Ball MJ. Topographic distribution of neurofibrillary tangles and granulovacuolar degeneration in hippocampal cortex of aging and demented patients. A quantitative study. Acta Neuropathol (Berl) 1978;42(2):73–80. [PubMed: 654888]
3. Basser PJ. Inferring microstructural features and the physiological state of tissues from diffusion-weighted images. NMR Biomed 1995;8(7–8):333–344. [PubMed: 8739270]
4. Basser PJ. New histological and physiological stains derived from diffusion-tensor MR images. Ann N Y Acad Sci 1997;820:123–138. [PubMed: 9237452]
5. Basser PJ, Mattiello J, LeBihan D. Estimation of the effective self-diffusion tensor from the NMR spin echo. J Magn Reson B 1994;103(3):247–254. [PubMed: 8019776]
6. Basser PJ, Pierpaoli C. Microstructural and physiological features of tissues elucidated by quantitative-diffusion-tensor MRI. J Magn Reson B 1996;111(3):209–219. [PubMed: 8661285]
7. Blessed G, Tomlinson BE, Roth M. The association between quantitative measures of dementia and of senile change in the cerebral grey matter of elderly subjects. Br J Psychiatry 1968;114(512):797–811. [PubMed: 5662937]
8. Bozzali M, Falini A, Franceschi M, Cercignani M, Zuffi M, Scotti G, Comi G, Filippi M. White matter damage in Alzheimer's disease assessed in vivo using diffusion tensor magnetic resonance imaging. J Neurol Neurosurg Psychiatry 2002;72(6):742–746. [PubMed: 12023417]
9. Braak H, Braak E. Neuropathological stageing of Alzheimer-related changes. Acta Neuropathol (Berl) 1991;82(4):239–259. [PubMed: 1759558]

10. Brun A, Englund E. A white matter disorder in dementia of the Alzheimer type: a pathoanatomical study. Ann Neurol 1986;19(3):253–262. [PubMed: 3963770]
11. Budde MD, Kim JH, Liang HF, Schmidt RE, Russell JH, Cross AH, Song SK. Toward accurate diagnosis of white matter pathology using diffusion tensor imaging. Magn Reson Med 2007;57(4): 688–695. [PubMed: 17390365]
12. Cavanna AE, Trimble MR. The precuneus: a review of its functional anatomy and behavioural correlates. Brain 2006;129(Pt 3):564–583. [PubMed: 16399806]
13. Chen SQ, Kang Z, Hu XQ, Hu B, Zou Y. Diffusion tensor imaging of the brain in patients with Alzheimer's disease and cerebrovascular lesions. J Zhejiang Univ Sci B 2007;8(4):242–247. [PubMed: 17444598]
14. Choi SJ, Lim KO, Monteiro I, Reisberg B. Diffusion tensor imaging of frontal white matter microstructure in early Alzheimer's disease: a preliminary study. J Geriatr Psychiatry Neurol 2005;18(1):12–19. [PubMed: 15681623]
15. Daselaar SM, Fleck MS, Cabeza R. Triple dissociation in the medial temporal lobes: recollection, familiarity, and novelty. J Neurophysiol 2006;96(4):1902–1911. [PubMed: 16738210]
16. de Jager CA, Budge MM, Clarke R. Utility of TICS-M for the assessment of cognitive function in older adults. Int J Geriatr Psychiatry 2003;18(4):318–324. [PubMed: 12673608]
17. de Leeuw FE, Korf E, Barkhof F, Scheltens P. White matter lesions are associated with progression of medial temporal lobe atrophy in Alzheimer disease. Stroke 2006;37(9):2248–2252. [PubMed: 16902173]
18. Desikan RS, Segonne F, Fischl B, Quinn BT, Dickerson BC, Blacker D, Buckner RL, Dale AM, Maguire RP, Hyman BT, Albert MS, Killiany RJ. An automated labeling system for subdividing the human cerebral cortex on MRI scans into gyral based regions of interest. Neuroimage 2006;31(3):968–980. [PubMed: 16530430]
19. Englund E, Brun A. White matter changes in dementia of Alzheimer's type: the difference in vulnerability between cell compartments. Histopathology 1990;16(5):433–439. [PubMed: 2361659]
20. Englund E, Brun A, Alling C. White matter changes in dementia of Alzheimer's type. Biochemical and neuropathological correlates. Brain 1988;111(Pt 6):1425–1439. [PubMed: 3208064]
21. Englund E, Sjobeck M, Brockstedt S, Latt J, Larsson EM. Diffusion tensor MRI post mortem demonstrated cerebral white matter pathology. J Neurol 2004;251(3):350–352. [PubMed: 15015019]
22. Fischl B, Salat DH, Busa E, Albert M, Dieterich M, Haselgrove C, van der Kouwe A, Killiany R, Kennedy D, Klaveness S, Montillo A, Makris N, Rosen B, Dale AM. Whole brain segmentation: automated labeling of neuroanatomical structures in the human brain. Neuron 2002;33(3):341–355. [PubMed: 11832223]
23. Folstein MF, Folstein SE, McHugh PR. "Mini-mental state". A practical method for grading the cognitive state of patients for the clinician. J Psychiatr Res 1975;12(3):189–198. [PubMed: 1202204]
24. Fotenos AF, Snyder AZ, Girton LE, Morris JC, Buckner RL. Normative estimates of cross-sectional and longitudinal brain volume decline in aging and AD. Neurology 2005;64(6):1032–1039. [PubMed: 15781822]
25. Gomez-Isla T, Price JL, McKeel DW Jr, Morris JC, Growdon JH, Hyman BT. Profound loss of layer II entorhinal cortex neurons occurs in very mild Alzheimer's disease. J Neurosci 1996;16(14):4491–4500. [PubMed: 8699259]
26. Habeck M, Nilges M, Rieping W. Replica-exchange Monte Carlo scheme for bayesian data analysis. Phys Rev Lett 2005;94(1) 018105.
27. Han X, Jovicich J, Salat D, van der Kouwe A, Quinn B, Czanner S, Busa E, Pacheco J, Albert M, Killiany R, Maguire P, Rosas D, Makris N, Dale A, Dickerson B, Fischl B. Reliability of MRI-derived measurements of human cerebral cortical thickness: the effects of field strength, scanner upgrade and manufacturer. Neuroimage 2006;32(1):180–194. [PubMed: 16651008]
28. Head D, Buckner RL, Shimony JS, Williams LE, Akbudak E, Conturo TE, McAvoy M, Morris JC, Snyder AZ. Differential vulnerability of anterior white matter in nondemented aging with minimal

acceleration in dementia of the Alzheimer type: evidence from diffusion tensor imaging. Cereb Cortex 2004;14(4):410–423. [PubMed: 15028645]

29. Hirono N, Hashimoto M, Ishii K, Kazui H, Mori E. One-year change in cerebral glucose metabolism in patients with Alzheimer's disease. J Neuropsychiatry Clin Neurosci 2004;16(4): 488–492. [PubMed: 15616176]
30. Hirono N, Kitagaki H, Kazui H, Hashimoto M, Mori E. Impact of white matter changes on clinical manifestation of Alzheimer's disease: A quantitative study. Stroke 2000;31(9):2182–2188. [PubMed: 10978049]
31. Huang J, Friedland RP, Auchus AP. Diffusion tensor imaging of normal-appearing white matter in mild cognitive impairment and early Alzheimer disease: preliminary evidence of axonal degeneration in the temporal lobe. AJNR Am J Neuroradiol 2007;28(10):1943–1948. [PubMed: 17905894]
32. Hughes CP, Berg L, Danziger WL, Coben LA, Martin RL. A new clinical scale for the staging of dementia. Br J Psychiatry 1982;140:566–572. [PubMed: 7104545]
33. Hyman BT, Van Hoesen GW, Damasio AR, Barnes CL. Alzheimer's disease: cell-specific pathology isolates the hippocampal formation. Science 1984;225(4667):1168–1170. [PubMed: 6474172]
34. Hyman BT, Van Hoesen GW, Kromer LJ, Damasio AR. Perforant pathway changes and the memory impairment of Alzheimer's disease. Ann Neurol 1986;20(4):472–481. [PubMed: 3789663]
35. Ishii K, Kawachi T, Sasaki H, Kono AK, Fukuda T, Kojima Y, Mori E. Voxel-based morphometric comparison between early- and late-onset mild Alzheimer's disease and assessment of diagnostic performance of z score images. AJNR Am J Neuroradiol 2005;26(2):333–340. [PubMed: 15709131]
36. Jack CR Jr, Petersen RC, O'Brien PC, Tangalos EG. MR-based hippocampal volumetry in the diagnosis of Alzheimer's disease. Neurology 1992;42(1):183–188. [PubMed: 1734300]
37. Jenkinson M, Bannister P, Brady M, Smith S. Improved optimization for the robust and accurate linear registration and motion correction of brain images. Neuroimage 2002;17(2):825–841. [PubMed: 12377157]
38. Jernigan TL, Salmon DP, Butters N, Hesselink JR. Cerebral structure on MRI, Part II: Specific changes in Alzheimer's and Huntington's diseases. Biol Psychiatry 1991;29(1):68–81. [PubMed: 1825793]
39. Jones DK, Horsfield MA, Simmons A. Optimal strategies for measuring diffusion in anisotropic systems by magnetic resonance imaging. Magn Reson Med 1999;42(3):515–525. [PubMed: 10467296]
40. Li TQ, Kim DH, Moseley ME. High-resolution diffusion-weighted imaging with interleaved variable-density spiral acquisitions. J Magn Reson Imaging 2005;21(4):468–475. [PubMed: 15779030]
41. Lipton RB, Katz MJ, Kuslansky G, Sliwinski MJ, Stewart WF, Verghese J, Crystal HA, Buschke H. Screening for dementia by telephone using the memory impairment screen. J Am Geriatr Soc 2003;51(10):1382–1390. [PubMed: 14511157]
42. Liu C, Bammer R, Kim DH, Moseley ME. Self-navigated interleaved spiral (SNAILS): application to high-resolution diffusion tensor imaging. Magn Reson Med 2004;52(6):1388–1396. [PubMed: 15562493]
43. Liu C, Moseley ME, Bammer R. Simultaneous phase correction and SENSE reconstruction for navigated multi-shot DWI with non-cartesian k-space sampling. Magn Reson Med 2005;54(6): 1412–1422. [PubMed: 16276497]
44. Lustig C, Snyder AZ, Bhakta M, O'Brien KC, McAvoy M, Raichle ME, Morris JC, Buckner RL. Functional deactivations: change with age and dementia of the Alzheimer type. Proc Natl Acad Sci U S A 2003;100(24):14504–14509. [PubMed: 14608034]
45. Medina D, DeToledo-Morrell L, Urresta F, Gabrieli JD, Moseley M, Fleischman D, Bennett DA, Leurgans S, Turner DA, Stebbins GT. White matter changes in mild cognitive impairment and AD: A diffusion tensor imaging study. Neurobiol Aging 2006;27(5):663–672. [PubMed: 16005548]

46. Mintun MA, Larossa GN, Sheline YI, Dence CS, Lee SY, Mach RH, Klunk WE, Mathis CA, DeKosky ST, Morris JC. [11C]PIB in a nondemented population: potential antecedent marker of Alzheimer disease. Neurology 2006;67(3):446–452. [PubMed: 16894106]
47. Mohedano-Moriano A, Pro-Sistiaga P, Arroyo-Jimenez MM, Artacho-Perula E, Insausti AM, Marcos P, Cebada-Sanchez S, Martinez-Ruiz J, Munoz M, Blaizot X, Martinez-Marcos A, Amaral DG, Insausti R. Topographical and laminar distribution of cortical input to the monkey entorhinal cortex. J Anat 2007;211(2):250–260. [PubMed: 17573826]
48. Morris JC. Clinical dementia rating: a reliable and valid diagnostic and staging measure for dementia of the Alzheimer type. Int Psychogeriatr 1997;9 Suppl 1:173–176. discussion 7–8. [PubMed: 9447441]
49. Morris JC, Ernesto C, Schafer K, Coats M, Leon S, Sano M, Thal LJ, Woodbury P. Clinical dementia rating training and reliability in multicenter studies: the Alzheimer's Disease Cooperative Study experience. Neurology 1997;48(6):1508–1510. [PubMed: 9191756]
50. Moseley M. Diffusion tensor imaging and aging - a review. NMR Biomed 2002;15(7–8):553–560. [PubMed: 12489101]
51. Mungas D, Harvey D, Reed BR, Jagust WJ, DeCarli C, Beckett L, Mack WJ, Kramer JH, Weiner MW, Schuff N, Chui HC. Longitudinal volumetric MRI change and rate of cognitive decline. Neurology 2005;65(4):565–571. [PubMed: 16116117]
52. Park HJ, Kubicki M, Shenton ME, Guimond A, McCarley RW, Maier SE, Kikinis R, Jolesz FA, Westin CF. Spatial normalization of diffusion tensor MRI using multiple channels. Neuroimage 2003;20(4):1995–2009. [PubMed: 14683705]
53. Pfefferbaum A, Adalsteinsson E, Sullivan EV. Frontal circuitry degradation marks healthy adult aging: Evidence from diffusion tensor imaging. Neuroimage 2005;26(3):891–899. [PubMed: 15955499]
54. Pfefferbaum A, Sullivan EV. Increased brain white matter diffusivity in normal adult aging: relationship to anisotropy and partial voluming. Magn Reson Med 2003;49(5):953–961. [PubMed: 12704779]
55. Pfefferbaum A, Sullivan EV, Hedehus M, Lim KO, Adalsteinsson E, Moseley M. Age-related decline in brain white matter anisotropy measured with spatially corrected echo-planar diffusion tensor imaging. Magn Reson Med 2000;44(2):259–268. [PubMed: 10918325]
56. Pierpaoli C, Basser PJ. Toward a quantitative assessment of diffusion anisotropy. Magn Reson Med 1996;36(6):893–906. [PubMed: 8946355]
57. Prins ND, van Dijk EJ, den Heijer T, Vermeer SE, Koudstaal PJ, Oudkerk M, Hofman A, Breteler MM. Cerebral white matter lesions and the risk of dementia. Arch Neurol 2004;61(10):1531–1534. [PubMed: 15477506]
58. Reese TG, Heid O, Weisskoff RM, Wedeen VJ. Reduction of eddy-current-induced distortion in diffusion MRI using a twice-refocused spin echo. Magn Reson Med 2003;49(1):177–182. [PubMed: 12509835]
59. Rieping W, Habeck M, Nilges M. Inferential structure determination. Science 2005;309(5732):303–306. [PubMed: 16002620]
60. Rombouts SA, Barkhof F, Goekoop R, Stam CJ, Scheltens P. Altered resting state networks in mild cognitive impairment and mild Alzheimer's disease: an fMRI study. Hum Brain Mapp 2005;26(4):231–239. [PubMed: 15954139]
61. Rose SE, Chen F, Chalk JB, Zelaya FO, Strugnell WE, Benson M, Semple J, Doddrell DM. Loss of connectivity in Alzheimer's disease: an evaluation of white matter tract integrity with colour coded MR diffusion tensor imaging. J Neurol Neurosurg Psychiatry 2000;69(4):528–530. [PubMed: 10990518]
62. Rose SE, McMahon KL, Janke AL, O'Dowd B, de Zubicaray G, Strudwick MW, Chalk JB. Diffusion indices on magnetic resonance imaging and neuropsychological performance in amnestic mild cognitive impairment. J Neurol Neurosurg Psychiatry 2006;77(10):1122–1128. [PubMed: 16754694]
63. Rueckert D, Sonoda LI, Hayes C, Hill DL, Leach MO, Hawkes DJ. Nonrigid registration using free-form deformations: application to breast MR images. IEEE Trans Med Imaging 1999;18(8):712–721. [PubMed: 10534053]

64. Salat DH, Kaye JA, Janowsky JS. Prefrontal gray and white matter volumes in healthy aging and Alzheimer disease. Arch Neurol 1999;56(3):338–344. [PubMed: 10190825]
65. Salat DH, Kaye JA, Janowsky JS. Selective preservation and degeneration within the prefrontal cortex in aging and Alzheimer disease. Arch Neurol 2001;58(9):1403–1408. [PubMed: 11559311]
66. Salat DH, Stangl PA, Kaye JA, Janowsky JS. Sex differences in prefrontal volume with aging and Alzheimer's disease. Neurobiol Aging 1999;20(6):591–596. [PubMed: 10674424]
67. Salat DH, Tuch DS, Greve DN, van der Kouwe AJ, Hevelone ND, Zaleta AK, Rosen BR, Fischl B, Corkin S, Rosas HD, Dale AM. Age-related alterations in white matter microstructure measured by diffusion tensor imaging. Neurobiol Aging 2005;26(8):1215–1227. [PubMed: 15917106]
68. Salat DH, Tuch DS, Hevelone ND, Fischl B, Corkin S, Rosas HD, Dale AM. Age-related changes in prefrontal white matter measured by diffusion tensor imaging. Ann N Y Acad Sci 2005;1064:37–49. [PubMed: 16394146]
69. Schmahmann, J.; Pandya, D. Fiber Pathways of the Brain. Oxford: Oxford University Press; 2006.
70. Schmidt R, Schmidt H, Kapeller P, Enzinger C, Ropele S, Saurugg R, Fazekas F. The natural course of MRI white matter hyperintensities. J Neurol Sci 2002;203–204:253–257.
71. Sjobeck M, Haglund M, Englund E. White matter mapping in Alzheimer's disease: A neuropathological study. Neurobiol Aging 2006;27(5):673–680. [PubMed: 15894407]
72. Smith SM, Jenkinson M, Johansen-Berg H, Rueckert D, Nichols TE, Mackay CE, Watkins KE, Ciccarelli O, Cader MZ, Matthews PM, Behrens TE. Tract-based spatial statistics: voxelwise analysis of multi-subject diffusion data. Neuroimage 2006;31(4):1487–1505. [PubMed: 16624579]
73. Smith SM, Jenkinson M, Woolrich MW, Beckmann CF, Behrens TE, Johansen-Berg H, Bannister PR, De Luca M, Drobnjak I, Flitney DE, Niazy RK, Saunders J, Vickers J, Zhang Y, De Stefano N, Brady JM, Matthews PM. Advances in functional and structural MR image analysis and implementation as FSL. Neuroimage 2004;23 Suppl 1:S208–S219. [PubMed: 15501092]
74. Song SK, Sun SW, Ju WK, Lin SJ, Cross AH, Neufeld AH. Diffusion tensor imaging detects and differentiates axon and myelin degeneration in mouse optic nerve after retinal ischemia. Neuroimage 2003;20(3):1714–1722. [PubMed: 14642481]
75. Song SK, Sun SW, Ramsbottom MJ, Chang C, Russell J, Cross AH. Dysmyelination revealed through MRI as increased radial (but unchanged axial) diffusion of water. Neuroimage 2002;17(3):1429–1436. [PubMed: 12414282]
76. Stern Y, Hesdorffer D, Sano M, Mayeux R. Measurement and prediction of functional capacity in Alzheimer's disease. Neurology 1990;40(1):8–14. [PubMed: 2296387]
77. Stoub TR, deToledo-Morrell L, Stebbins GT, Leurgans S, Bennett DA, Shah RC. Hippocampal disconnection contributes to memory dysfunction in individuals at risk for Alzheimer's disease. Proc Natl Acad Sci U S A 2006;103(26):10041–10045. [PubMed: 16785436]
78. Stout JC, Jernigan TL, Archibald SL, Salmon DP. Association of dementia severity with cortical gray matter and abnormal white matter volumes in dementia of the Alzheimer type. Arch Neurol 1996;53(8):742–749. [PubMed: 8759980]
79. Sullivan EV, Adalsteinsson E, Hedehus M, Ju C, Moseley M, Lim KO, Pfefferbaum A. Equivalent disruption of regional white matter microstructure in ageing healthy men and women. Neuroreport 2001;12(1):99–104. [PubMed: 11201100]
80. Sullivan EV, Adalsteinsson E, Pfefferbaum A. Selective age-related degradation of anterior callosal fiber bundles quantified in vivo with fiber tracking. Cereb Cortex 2006;16(7):1030–1039. [PubMed: 16207932]
81. Sullivan EV, Pfefferbaum A. Diffusion tensor imaging and aging. Neurosci Biobehav Rev 2006;30(6):749–761. [PubMed: 16887187]
82. Swendsen RH, Wang JS. Replica Monte Carlo simulation of spin glasses. Physical Review Letters 1986;57(21):2607–2609. [PubMed: 10033814]
83. Taoka T, Iwasaki S, Sakamoto M, Nakagawa H, Fukusumi A, Myochin K, Hirohashi S, Hoshida T, Kichikawa K. Diffusion anisotropy and diffusivity of white matter tracts within the temporal stem in Alzheimer disease: evaluation of the "tract of interest" by diffusion tensor tractography. AJNR Am J Neuroradiol 2006;27(5):1040–1045. [PubMed: 16687540]
84. Tuch DS. Q-ball imaging. Magn Reson Med 2004;52(6):1358–1372. [PubMed: 15562495]

85. Tuch DS, Reese TG, Wiegell MR, Makris N, Belliveau JW, Wedeen VJ. High angular resolution diffusion imaging reveals intravoxel white matter fiber heterogeneity. Magn Reson Med 2002;48(4):577–582. [PubMed: 12353272]

86. Van Hoesen GW, Hyman BT, Damasio AR. Entorhinal cortex pathology in Alzheimer's disease. Hippocampus 1991;1(1):1–8. [PubMed: 1669339]

87. Vincent JL, Snyder AZ, Fox MD, Shannon BJ, Andrews JR, Raichle ME, Buckner RL. Coherent spontaneous activity identifies a hippocampal-parietal memory network. J Neurophysiol 2006;96(6):3517–3531. [PubMed: 16899645]

88. Walhovd KB, Fjell AM, Reinvang I, Lundervold A, Dale AM, Eilertsen DE, Quinn BT, Salat D, Makris N, Fischl B. Effects of age on volumes of cortex, white matter and subcortical structures. Neurobiol Aging 2005;26(9):1261–1270. discussion 75–8. [PubMed: 16005549]

89. Wang L, Zang Y, He Y, Liang M, Zhang X, Tian L, Wu T, Jiang T, Li K. Changes in hippocampal connectivity in the early stages of Alzheimer's disease: evidence from resting state fMRI. Neuroimage 2006;31(2):496–504. [PubMed: 16473024]

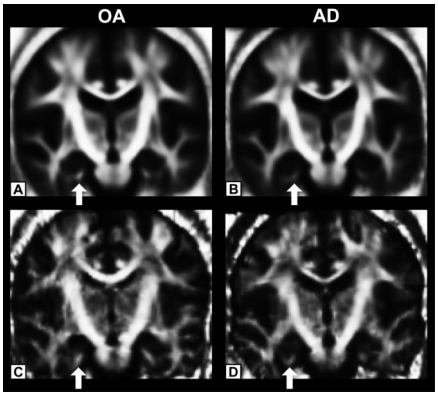

Figure 1.

Top panel. Example of a mean FA map in nondemented older adults (A) and patients with AD (B) resulting from the spatial normalization of the FA volumes using the IRTK nonlinear registration procedure [63] (http://www.doc.ic.ac.uk/~dr/software) from tract-based spatial statistics (TBSS) [72]. Bottom panel. Example of an individual FA map in a nondemented older adult (C) and in a patient with AD (D). Importantly, much of the anatomic detail in the individual participant volumes is retained in the group averaged volumes, and these averages do not qualitatively differ substantially between the control and AD groups, demonstrating the robustness of the nonlinear procedure. Alterations in parahippocampal FA can be qualitatively seen in the group average as well as in the individual participant comparison (reduced FA intensity between groups at the white arrows).

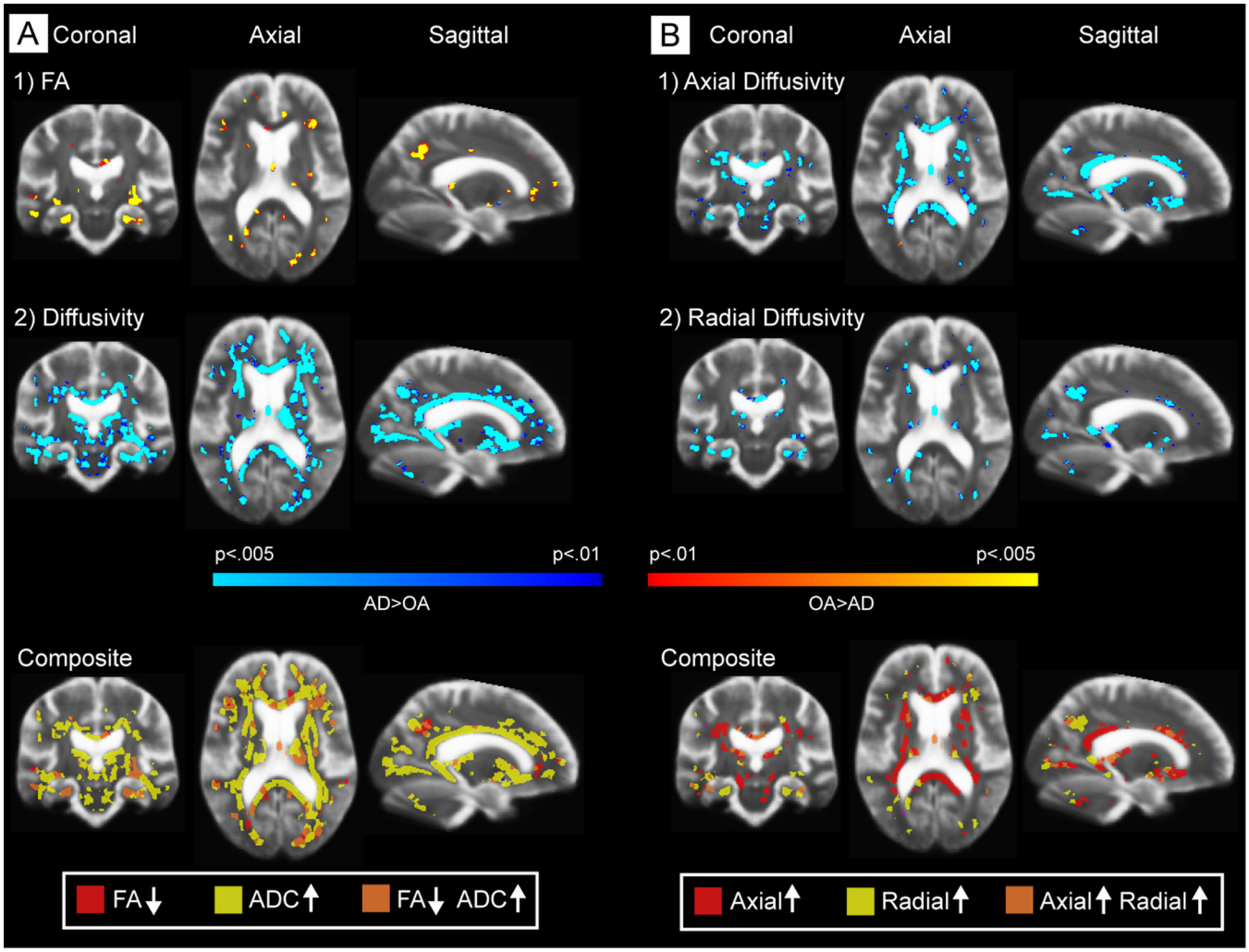

Figure 2.

TBSS-based statistical comparison of FA and diffusivity between OA and AD, regressing out T2 signal intensity. Left Panel. When controlling for T2 intensity, changes in FA were most prominent in parahippocampal, temporal, precuneus, and ventromedial frontal WM. Diffusivity increased with AD in regions similar to those reported for FA yet somewhat more widespread with additional changes in the corpus callosum, cingulum, occipital, and periventricular regions. Composite map of the statistical patterns of diffusion changes with group comparisons (bottom panel). Classes were distinguished based on the unique combination of each direction of the statistical results for each map for any results with a *p* value of 0.01 or lower (i.e. an increase or a decrease [2 classes] in FA or diffusivity and each potential unique combination of classes). Overlap in FA and diffusivity changes (results with a *p* value of 0.01 or lower) was greatest in medial temporal, precuneus, and ventromedial frontal WM (bottom left panel). Analyses controlled for T2 intensity at each voxel, and therefore the changes measured exceeded those of T2 which would be affected by partial volume and/or WM hyperintensities. Right Panel. Alterations in axial (right top) and radial (right middle) diffusivity in AD, and the composite of these effects (right bottom).

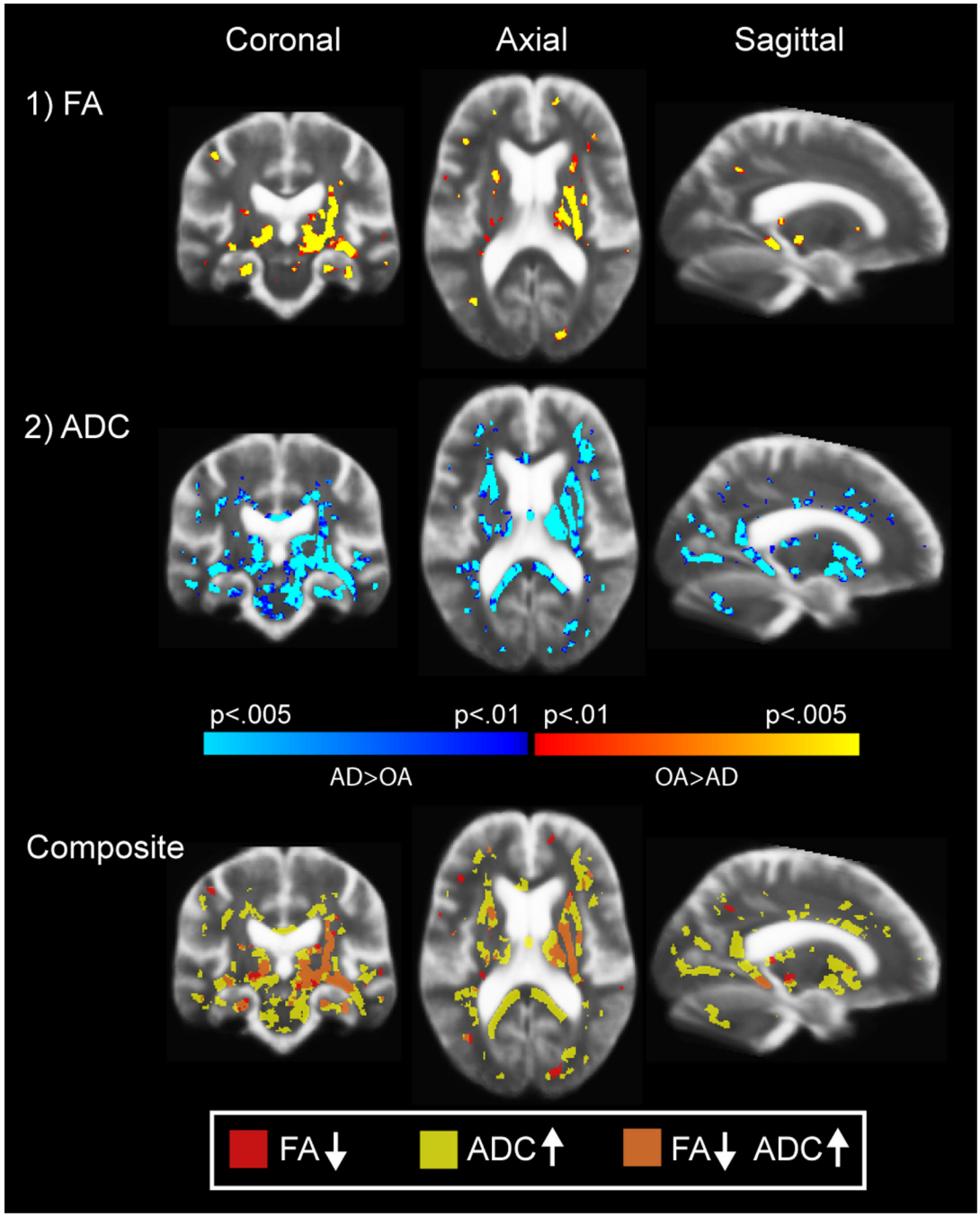

Figure 3.

TBSS-based statistical comparison of FA and diffusivity between OA and AD, regressing out T2 signal intensity and hippocampal volume. Hippocampal volume was treated as a nuisance covariate to determine whether there were effects of AD on diffusion parameters that were independent of this classical imaging measure of AD pathology. FA reductions with AD were prominent in medial temporal, temporal stem, and thalamic regions (top panel). Diffusivity changes were apparent throughout a number of ventral and periventricular WM areas (middle panel). Composite map of FA and diffusivity changes was greatest in temporal WM (bottom panel). Because hippocampal volume and T2 were both

treated as nuisance covariates, these results demonstrate the unique variance in diffusion parameters that is not explained by these other types of pathologic changes.

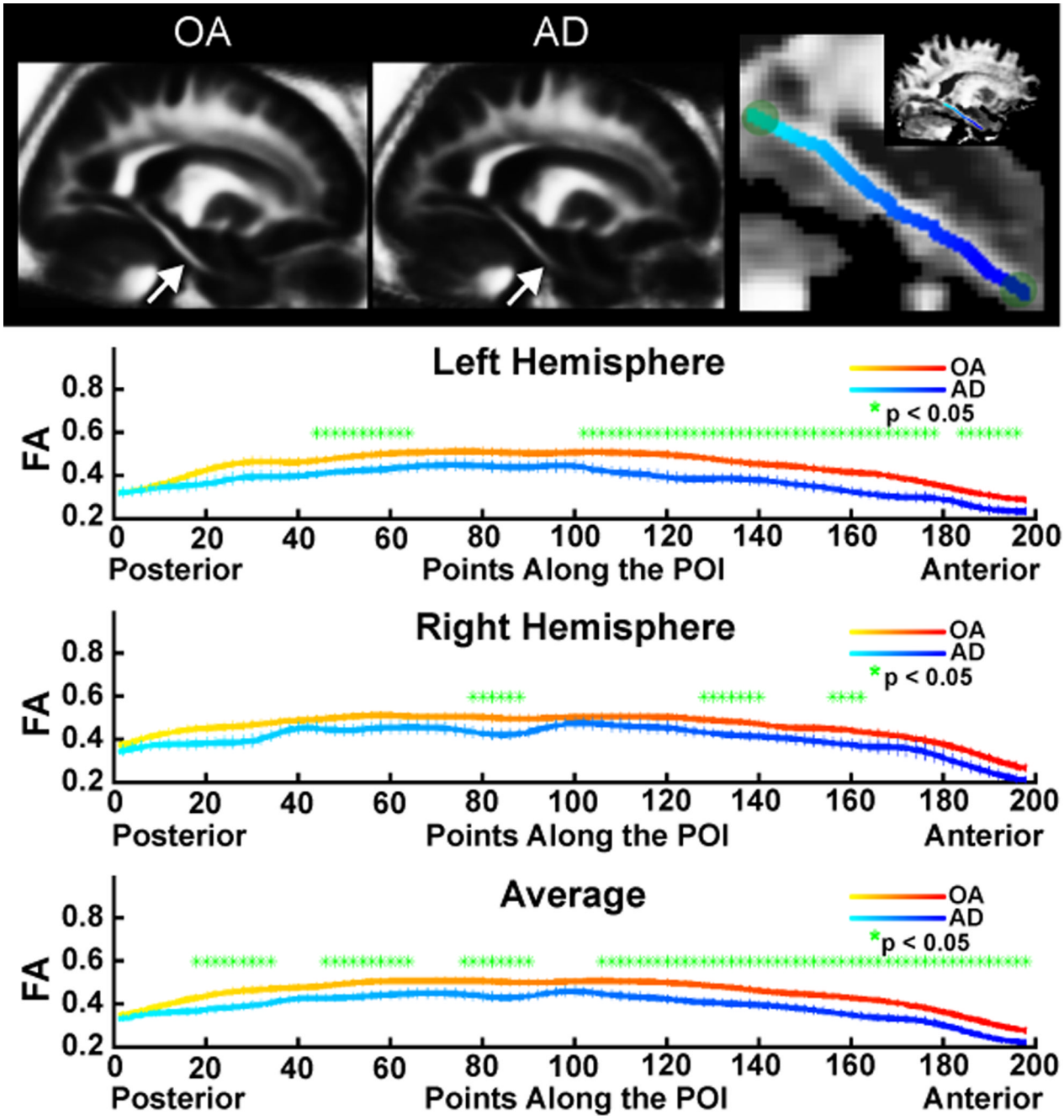

Figure 4.

Demonstration of the POI technique and analysis of parahippocampal WM. Seed points were manually placed in each individual participant's diffusion volumes at anterior and posterior points in the parahippocampal WM defined by morphometric landmarks in the T2 image. Those points were then connected using the optimal path calculated from the diffusion tensor information (top panel; see Methods). The mean of the OA (top left) and AD (top right) of a single sagittal is presented to demonstrate the visual differences in the raw data between these groups (arrows). FA was sampled from the central voxels along the path, providing an individual POI for each participant, and minimizing the potential confounds of partial volume contamination from more peripheral voxels. FA was most

affected in anterior portions of the parahippocampal WM, but significant reductions in FA were found with AD along the majority of the path when the mean FA across the hemispheres was examined (bottom plot). Overall path length did not differ between the groups.

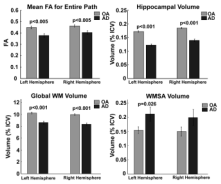

Figure 5.

Mean anisotropy along the entire path (top left) differed between OA and AD in the left and right hemispheres. For comparison, traditional imaging measures of AD pathology are presented including hippocampal volume (top right), total WM volume (bottom left), and white matter signal abnormality (WMSA; bottom right) volume.

Table 1

Participant Demographics

	OA	AD
N	54 (45F/9M)	20 (16F/4M)
Age	75.8 (5.6)	77.8 (4.9)
MMSE (n = 26)	28.8 (1.2)[a]	20.0 (5.4)[d]
BDS (n = 49)	0.86 (1.0)[b]	12.9 (6.4)
TICS (n = 22)	34.4 (2.0)[c]	NA
CDR Global (n = 20)	NA	11(.5)/7(1)/2(2)
CDR Sum of Boxes (n = 20)	NA	4.9 (2.9)

Data presented as mean and standard deviation where applicable.

MMSE, Mini Mental State Examination; BDS, Blessed Dementia Scale; TICS, Telephone Interview of Cognitive Status; CDR, Clinical Dementia Rating [32,48]; Higher scores indicate better performance on MMSE (0–30) and TICS (0–39), whereas lower scores indicate better performance on BDS (0–37), global CDR (0–3), and CDR sum of boxes (0–18).

[a] n=20

[b] n=29

[c] n=22

[d] n = 6

Table 2

Regions of altered FA in AD. Clusters with a p value of < 0.01 and a cluster size > 40 voxels.

Region	Size(mm^3)	Min p (10^{-x})	Weight*
Temporal			
Lh-inferior/middle temporal	1467	5.81	8523.30
Lh-parahippocampal	534	5.41	2888.90
Rh-middle temporal	502	4.75	2384.50
Rh-fusiform/inferior temporal/middle temporal	579	3.81	2206.00
Lh-medial temporal pole	358	4.66	1668.30
Lh-middle temporal	270	4.70	1269.00
Rh-temporal stem	304	3.28	997.12
Rh-inferior temporal	204	4.16	848.64
Rh-inferior temporal	181	3.97	718.57
Rh-middle temporal	170	3.98	676.60
Rh-parahippocampal	131	4.44	581.64
Lh-fusiform	161	−3.43	552.23
Lh-parahippocampal	87	3.71	322.77
Parietal			
Lh-precuneus	1219	4.18	5095.40
Lh-inferior parietal	620	4.74	2938.80
Lh-inferiorparietal/supramarginal	446	4.80	2140.80
Rh-supramarginal	366	3.59	1313.90
Lh-cuneus/precuneus	274	4.69	1285.10
Rh-precuneus	343	3.32	1138.80
Rh-inferior parietal	231	4.03	930.93
Lh-inferior parietal	176	4.48	788.48
Rh-precuneus	108	3.16	341.28
Lh-inferior parietal	109	3.07	334.63
Lh-precuneus	90	3.62	325.80
Frontal			
Rh-medial/lateral orbitofrontal	421	3.71	1561.90
Rh-superior frontal	181	4.30	778.30
Lh-rostral middle frontal,	89	3.66	325.74
Occipital			
Lh-lateral occipital/lingual	851	4.58	3897.60
Rh-lateraloccipital	516	5.78	2982.50
Deep/Other			
Lh-periventricular	1046	−5.00	5230.00
Lh-pulvinar	433	5.68	2459.40
Fornix	269	4.73	1272.40
Lh-anterior callosum	271	3.04	823.84
Rh-anterior capsule	210	3.02	634.20
Rh-pulvinar	133	4.71	626.43

Region Temporal	Size(mm^3)	Min p (10^{-x})	Weight*
Lh-posterior callosum	151	3.16	477.16
Rh-cerebellum	97	4.21	408.37
Lh-ventral diencephalons	83	3.80	315.40

*Regions were ordered by region/lobe and by a weighting calculated as the product of the cluster size by the minimum p value (expressed as 10^{-x}). The final weighting was somewhat arbitrary due to specifics of the processing procedures. Clusters with < 300 weight were omitted from the table. Regional definitions were based on proximity to neural labels described in [18,22].